http://dx.doi.org/10.1595/205651318X696800 *Johnson Matthey Technol. Rev.*, 2018, **62**, (2), 189–203

JOHNSON MATTHEY
TECHNOLOGY REVIEW
www.technology.matthey.com

Effect of Temperature and Catholyte Concentration on the Performance of a Chemically Regenerative Fuel Cell

POM-based catholytes for platinum-free polymer electrolyte fuel cells

By David B. Ward, Trevor J. Davies*#
Department of Natural Sciences, Faculty of Science & Engineering, University of Chester, Thornton Science Park, Pool Lane, Ince, Chester CH2 4NU, UK

***Email:** trevor.davies@ineos.com

#Present address: Electrochemical Technology Technical Centre, INOVYN, South Parade, Runcorn, Cheshire WA7 4JE, UK

Chemically regenerative redox cathode (CRRC) polymer electrolyte fuel cells (PEFCs) are attracting more interest as a platinum-free PEFC technology. These fuel cells utilise a liquid catalyst or catholyte, to perform the indirect reduction of oxygen, eliminating the major degradation mechanisms that plague PEFC durability. A key component of a CRRC PEFC system is the catholyte. This article reports a thorough study of the effect of catholyte concentration and temperature on CRRC PEFC system performance for $H_7PV_4Mo_8O_{40}$ and $Na_4H_3PV_4Mo_8O_{40}$, two promising polyoxometalate (POM)-based catholytes. The results suggest 80°C and a catholyte concentration of 0.3 M provide the optimum performance for both $H_7PV_4Mo_8O_{40}$ and $Na_4H_3PV_4Mo_8O_{40}$ (for ambient pressure operation).

1. Introduction

For decades, PEFCs have been promoted as the future replacement for power generation *via* fossil fuel combustion for both transport and stationary applications (1, 2). Despite the recent dominance of lithium-ion batteries in the 'electrochemical power' sector, hydrogen PEFCs are beginning to make a market impact, for example, with the launch of the Toyota Mirai and the increasing uptake of PEFCs in the materials handling sector (3, 4). In addition, governments are beginning the transition to a hydrogen economy, with Germany having the most ambitious target of 400 hydrogen refuelling stations by 2023 (5). However, issues around cost and durability have plagued PEFC development and continue to inhibit their widespread commercialisation (6).

In a conventional PEFC, hydrogen is oxidised to protons and electrons at the anode (Equation (i)) and oxygen (in air) is reduced to water at the cathode (Equation (ii)):

$$H_2 \rightarrow 2H^+ + 2e^- \quad \text{(i)}$$

$$O_2 + 4e^- + 4H^+ \rightarrow 2H_2O \quad \text{(ii)}$$

Overall:

$$2H_2 + O_2 \rightarrow 2H_2O \quad \text{(iii)}$$

The main cause of the cost and durability issues with conventional PEFCs is the direct four-electron reduction of oxygen at the cathode (Equation (ii)). Due to relatively slow kinetics (1, 7), high Pt loadings are required to catalyse the oxygen reduction reaction (ORR), increasing the cost of the membrane electrode assembly (MEA) (8). Up to 80% of the Pt in a conventional fuel cell can be on the cathode. Furthermore, the large overpotential required to induce the oxygen reduction reaction (even with high Pt loading) typically results in a

200 mV drop in operating voltage at relatively low current densities of ~0.2 A cm^{-2} (9). The presence of air at the cathode is also the key component in the major mechanisms of fuel cell degradation, including chemical degradation of membranes *via* peroxide species (10, 11) and voltage transients at cell start-up and shut-down that oxidise the catalyst's carbon support (12, 13).

An alternative solution to the problem of cost and durability is the CRRC PEFC, illustrated in **Figure 1**. These systems utilise the indirect reduction of oxygen and resemble a hybrid of a fuel cell and flow battery (14). The anode is essentially identical to that of a conventional PEFC, with hydrogen gas oxidised to protons and electrons at a catalyst (Pt) coated membrane. At the cathode, a catholyte (Cath) is reduced at a two-phase liquid | electrode boundary. With facile kinetics, this electrochemical reaction utilises a low cost porous graphite electrode, replacing the requirement for Pt. The reduced catholyte (H-Cath) then travels to an air bubbling device called the 'regenerator', where oxygen is reduced to water and the catholyte is returned to its original oxidised state. Consequently, gaseous air never enters the cathode, eliminating the major PEFC degradation mechanisms. In addition, the catholyte ensures the membrane remains well hydrated, allowing the use of dry hydrogen.

A key component of a CRRC PEFC system is the catholyte, a redox active electrolyte that reacts with dioxygen in its reduced form. To maximise the cell operating voltage the catholyte should: (a) possess a high redox potential in its oxidised state, as close to 1.23 V *vs.* the standard hydrogen electrode as possible; and (b) display fast regeneration kinetics (i.e. the chemical reaction between oxygen and the reduced catholyte) to ensure the catholyte is highly oxidised when leaving the regenerator. Tolmachev and Vorotyntsev recently published a thorough review of CRRC PEFCs (14), with a focus on all catholyte chemistries researched since the CRRC concept was first proposed by Posner in 1955 (15). At present, three aqueous catholyte chemistries dominate CRRC research and development. These are P-V-Mo POMs that utilise $V^{4+/5+}$ redox chemistry (16–18); $Fe^{2+/3+}$ systems with organic ligands selected to enhance the rate of the re-oxidation reaction (19); and an adaptation of the Otswald process exploiting NO/NO_3^- redox chemistry (20). **Table I** lists the best CRRC PEFC performance obtained to date with the three different catholyte chemistries. Transient peak power refers to the performance of the cell whereas steady state peak power is associated with the whole CRRC system (i.e. regenerator + cell) (16). Given the US Department of Energy (DOE) 2020 target for peak power in transportation PEFCs is 1000 mW cm^{-2} (21), the data in **Table I** suggests CRRC PEFCs could soon compete with conventional fuel cells.

In terms of power density, the most promising catholyte formulations are the POMs: $H_7PV_4Mo_8O_{40}$ for transient operation and $Na_4H_3PV_4Mo_8O_{40}$ for steady state operation (18). Furthermore, these catholytes are associated with excellent durability. Using 0.3 M $Na_4H_3PV_4Mo_8O_{40}$ in a single cell CRRC PEFC system, Ward *et al.* recently reported 200 hours operation (at constant current) with

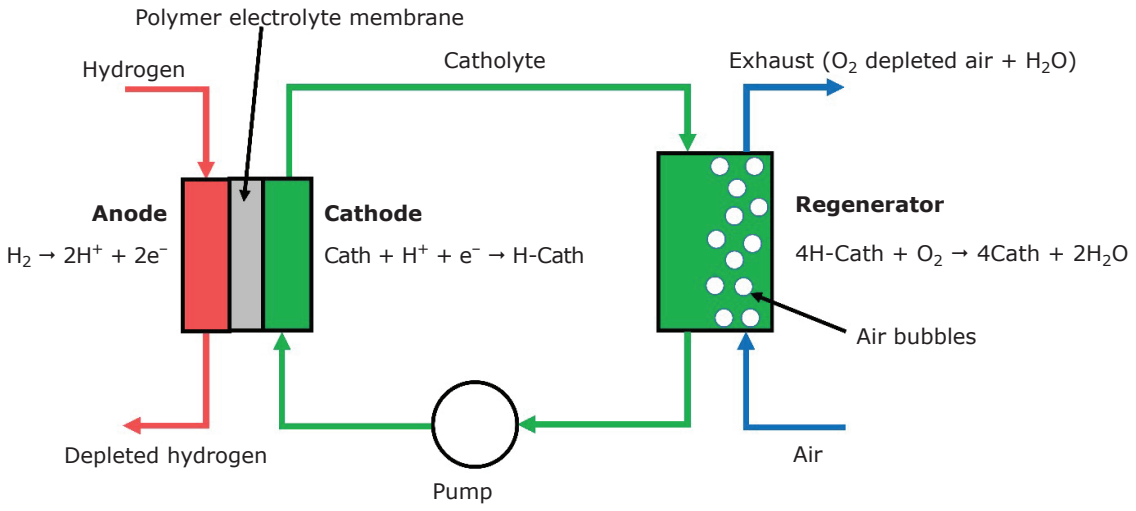

Fig. 1. Schematic diagram of a CRRC PEFC system with a hydrogen anode

Table I Details of Best Performing CRRC PEFC Systems Reported to Date (with H_2 as the Fuel)[a]

Catholyte	Cathode reaction (simplified)	Transient maximum power, mW cm^{-2}	Steady state maximum power, mW cm^{-2}	Reference
0.5 M $FeSO_4$ / 1 M H_2SO_4 / iron phthalocyanine	$Fe^{3+} + e^- \rightarrow Fe^{2+}$	249	–	(19)
5 M HNO_3	$2\ HNO_3 + 6\ H^+ + 6\ e^- \rightarrow 2\ NO(g) + 4\ H_2O$	730	–	(20)
0.45 M POM[b]	–	510	–	(17)
0.3 M $H_6PV_3Mo_9O_{40}$	$V^{5+} + e^- \rightarrow V^{4+}$	1000	380	(16)
0.3 M $H_7PV_4Mo_8O_{40}$	$V^{5+} + e^- \rightarrow V^{4+}$	1078	566	(18)
0.3 M $Na_4H_3PV_4Mo_8O_{40}$	$V^{5+} + e^- \rightarrow V^{4+}$	864	578	(18)

[a]All catholytes are aqueous

[b]Undisclosed polyoxometalate

negligible loss in performance (18). Indeed, a similar system was almost commercialised by ACAL Energy Ltd, UK, who achieved over 10,000 hours operation on an automotive test cycle without any significant signs of degradation (22). In their fully oxidised forms, the vanadium and molybdenum POM constituents have oxidation states +5 and +6, respectively. Upon electrochemical reduction in the cell, vanadium(V) is reduced to vanadium(IV) whilst the molybdenum remains unchanged (23). As such, a reduction level of 100% corresponds to a catholyte where the vanadium and molybdenum have oxidation states +4 and +6, respectively (the reduction of molybdenum occurs at lower potentials). Under most operating conditions, the catholytes are partially reduced, with a mixture of vanadium(V) and vanadium(IV). Upon contact with oxygen, the vanadium(IV) is chemically oxidised to vanadium(V) and O_2 is reduced to water, regenerating the catholyte for its next visit to the cell.

Little is known regarding the effect of concentration and temperature on CRRC PEFC systems using $H_7PV_4Mo_8O_{40}$ and $Na_4H_3PV_4Mo_8O_{40}$ catholytes, with 0.3 M and 80°C the only reported parameters (18). Matsui *et al.* studied the effect of concentration and temperature on the performance of a similar catholyte, $H_6PV_3Mo_9O_{40}$ (24). They found a concentration of 0.3 M and a system temperature of 80°C gave the best performance. However, the two values were the limits of their test matrix and the cell performance achieved was relatively poor compared to a study with the same catholyte (16). In this article, we report the study of a larger temperature-concentration matrix using the best CRRC catholytes in the literature, $H_7PV_4Mo_8O_{40}$ and $Na_4H_3PV_4Mo_8O_{40}$. Catholyte concentration ranges from 0.2 M to 0.45 M and temperature from 40°C to 90°C (at ambient pressure). High temperature operation (i.e. above 80°C) is desirable as it has been shown to improve peak power density in both conventional fuel cells and flow batteries (25, 26). In addition, operating PEFCs above 80°C provides heat management and CO tolerance benefits (27).

2. Experimental Details

A brief description of the experimental equipment and procedures is provided below, with more details in the Supplementary Information.

$H_7PV_4Mo_8O_{40}$ catholyte (HV4) synthesis followed the 'Metallomax' procedure (28) using the reagents: deionised water (with a resistivity of 18.2 MΩ cm); vanadium(V) oxide (V_2O_5) powder (99.2%, Alfa Aesar, UK); Mo powder (99.9%, Alfa Aesar, UK); phosphoric acid (H_3PO_4) (85.0%, Sigma Aldrich, UK); and molybdenum trioxide (MoO_3) (99.5%, Alfa Aesar, UK). $Na_4H_3PV_4Mo_8O_{40}$ catholyte (NaV4) was produced from HV4 by the addition of NaOH (98%, Alfa Aesar, UK). Catholyte concentration was determined gravimetrically using 25 ml glass density jars and pre-determined density *vs.* concentration calibration curves. Adjustment was achieved by either deionised water addition or heating and evaporation as required. The matrix of concentrations and temperatures studied (for both HV4 and NaV4) is given in **Table II**.

The cell components and build procedure (single cell, 5 × 5 cm active area) were identical

Table II Temperature and Catholyte Concentration Values Investigated (for both HV4 and NaV4)

Temperature, °C	Catholyte concentration, M			
	0.2	0.3	0.4	0.45
40	✓	✓		✓
50		✓		
60		✓		
70		✓		
80	✓	✓	✓	✓
90	✓	✓		✓

to that reported previously (16), apart from the membrane electrode assemblies. The latter were NR212 membranes with a 'standard' anode catalyst coating (0.3 mg Pt cm^{-2}) and a naked cathode side (supplied by Ion Power GmbH, Munich, Germany). Although this is a thicker membrane than the previously used Gore Primea (resulting in poorer fuel cell performance), it was found to be robust to large temperature variations and gave more repeatable results.

The CRRC test rig and experimental procedures were identical to those reported previously (16). All cell tests were conducted using a catholyte flow rate of 140 ml min^{-1} and air flow rate of 1 l min^{-1} (into the regenerator at ambient pressure). The anode hydrogen pressure was 1 bar and the cell was operated 'dead-ended' with occasional hydrogen purge events to remove excess water. The cell temperature was controlled using heating rods (RS, UK) inserted in the steel end plates whilst the catholyte temperature was controlled with a CAST-X 300 inline heater (Cast Aluminum Solutions, USA). An HCP-803 potentiostat (Bio-Logic, France) was used for all cell current-voltage (I–V) curves, monitoring open circuit voltage and electrochemical impedance spectroscopy. All cell tests were repeated for a range of catholyte reduction levels apart from impedance measurements, which were only conducted with catholytes at reduction levels corresponding to fuel cell open circuit voltage values of 800 ± 25 mV (see the Supplementary Information for more details). All cell and rig components displayed good chemical compatibility with the POM catholytes and no degradation of components was observed throughout testing.

Catholyte conductivity and pH were measured using a pHenomenal CO1300L conductivity meter (VWR International, UK) and 827 pH Lab pH meter (Metrohm, UK). Catholyte redox potentials were measured using a mercurous sulfate reference electrode and a JP945 graphite rod (Merson UK) as a working electrode. Fully oxidised samples of all catholytes were submitted for ^{31}P nuclear magnetic resonance (NMR) analysis (more details in the Supplementary Information).

3. Results and Discussion

3.1 Catholyte Composition

Aqueous solutions of $H_{3+x}PV_xMo_{12-x}O_{40}$ where $x > 1$ contain a mixture of species in dynamic equilibrium (29–32). Typically, the vanadium is present in keggin anions or in its free form of VO_2^+ (vanadium(V)). Likewise, if the POM is reduced, vanadium(IV) can exist as keggin-bound or free VO^{2+}. To provide an indication of the speciation in the catholytes, fully oxidised samples underwent ^{31}P NMR analysis. Example spectra are given in the Supplementary Information. Peak analysis followed that of Pettersson and co-workers (30, 31), from which it was possible to estimate concentrations of different species: VO_2^+ (Free V); $PV_1Mo_{11}O_{40}$ keggins (V_1-keggin); $PV_2Mo_{10}O_{40}$ keggins (V_2-keggin); $PV_3Mo_9O_{40}$ keggins (V_3-keggin); $PV_4Mo_8O_{40}$ keggins (V_4-keggin); and free phosphate (phosphate). **Figure 2** illustrates the ^{31}P NMR speciation results for $Na_4H_3PV_4Mo_8O_{40}$ and $H_7PV_4Mo_8O_{40}$ across a range of concentrations at 298 K.

In general, increasing the catholyte concentration increases the concentration of all the species involved in the dynamic equilibrium. However, pH also plays a role, which is evident in the difference between NaV4 and HV4. For a given POM concentration, increasing the pH of the catholyte by adding NaOH to convert HV4 to NaV4 results in less free vanadium and more V_4- and V_3-keggins. This agrees with the equilibrium proposed by Souchay and co-workers (33) (Equation (iv)):

$$(13 - n)[H_{n-1}PV_nMo_{12-n}O_{40}]^{4-} + 16H^+ \leftrightarrows (12 - n)[H_{n-2}PV_{n-1}Mo_{13-n}O_{40}]^{4-} + 12VO_2^+ + H_3PO_4 + 12H_2O \quad (iv)$$

POM speciation plays a key role in the regeneration reaction. Reduced keggins containing three or more vanadium centres are the only species that react with oxygen at an appreciable rate (34–36). Thus, higher concentrations of V_3 and V_4-keggins are favourable and **Figure 2** suggests NaV4 should undergo faster regeneration than HV4.

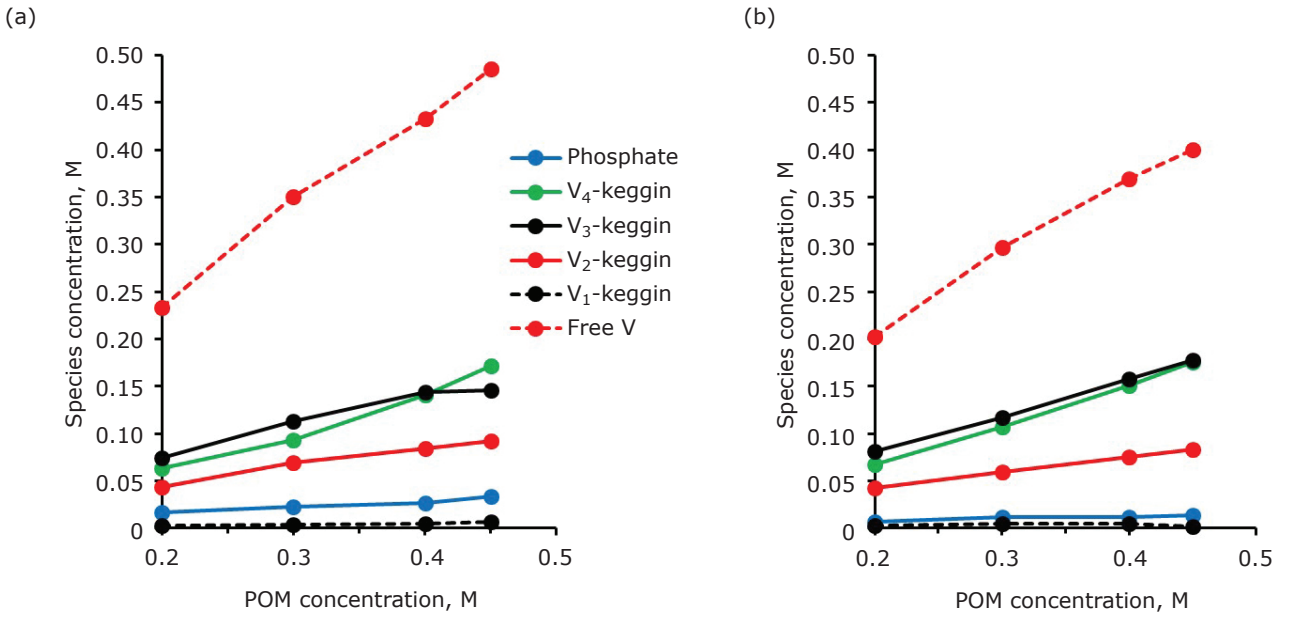

Fig. 2. Estimated concentrations of species present in fully oxidised samples at 298 K (determined from ^{31}P NMR) for: (a) HV4; (b) NaV4 in a range of catholyte (POM) concentrations

3.2 *Ex Situ* Thermodynamic Properties

Figures 3(a) and **3(b)** illustrate the effect of temperature and catholyte concentration on the redox potential of HV4 ($H_7PV_4Mo_8O_{40}$) and NaV4 ($Na_4H_3PV_4Mo_8O_{40}$) catholytes at a reduction level of 5% (i.e. 5% vanadium(IV), 95% vanadium(V)). Note, measured catholyte redox potentials correlate well with the corresponding CRRC cell open circuit voltages (OCV) (16). Similar results were achieved for a range of reduction levels. As seen previously (18), the protonic catholyte (HV4) has considerably higher redox potentials than its sodium analogue (a consequence of pH). For both catholytes, increasing temperature generally decreases the redox potential and consequently, the cell OCV. Concentration has the opposite effect. Further insights are provided by the pH measurements in **Figures 3(c)** and **3(d)**. Both catholytes contain free and keggin-bound vanadium. Free vanadium(V) undergoes a one-electron two-proton reduction, whereas keggin bound vanadium(V) reduction is thought to proceed *via* a one-electron one-proton mechanism (37) (Equations (v) and (vi)):

$$VO_2^+ + e^- + 2H^+ \leftrightarrow VO^{2+} + H_2O \quad (v)$$

$$[H_{n+m-1}PV^{IV}{}_mV^V{}_{n-m}Mo_{12-n}O_{40}]^{4-} + e^- + H^+ \leftrightarrow [H_{n+m}PV^{IV}{}_{m+1}V^V{}_{n-m-1}Mo_{12-n}O_{40}]^{4-} \quad (vi)$$

Thus, all the redox couples in the catholytes are pH sensitive and their redox potentials should increase as the pH decreases (i.e. a Nernstian relationship). This agrees with the trends observed in **Figures 3(b)** and **3(d)** – both catholytes are acids, so concentration has a strong effect on pH, leading to a positive correlation between proton concentration and redox potential. However, the subtle changes in pH with temperature do not follow the general decline in redox potential as temperature increases, suggesting speciation effects may play a role. The conductivity results in **Figures 3(e)** and **3(f)** are expected. Increasing temperature results in faster moving ions whilst increasing catholyte concentration increases the number of ions in the solution. Thus, increasing concentration should have a positive effect on cell performance, increasing the catholyte redox potential (and consequently cell OCV) and reducing the cell ohmic resistance, whereas the case for temperature is more complicated.

3.3 Cell Performance

Figures 4(a) and **4(b)** illustrate the transient cell performance of 5% reduced HV4 for a range of catholyte concentrations at 80°C (the same trends were observed for a range of reduction levels).

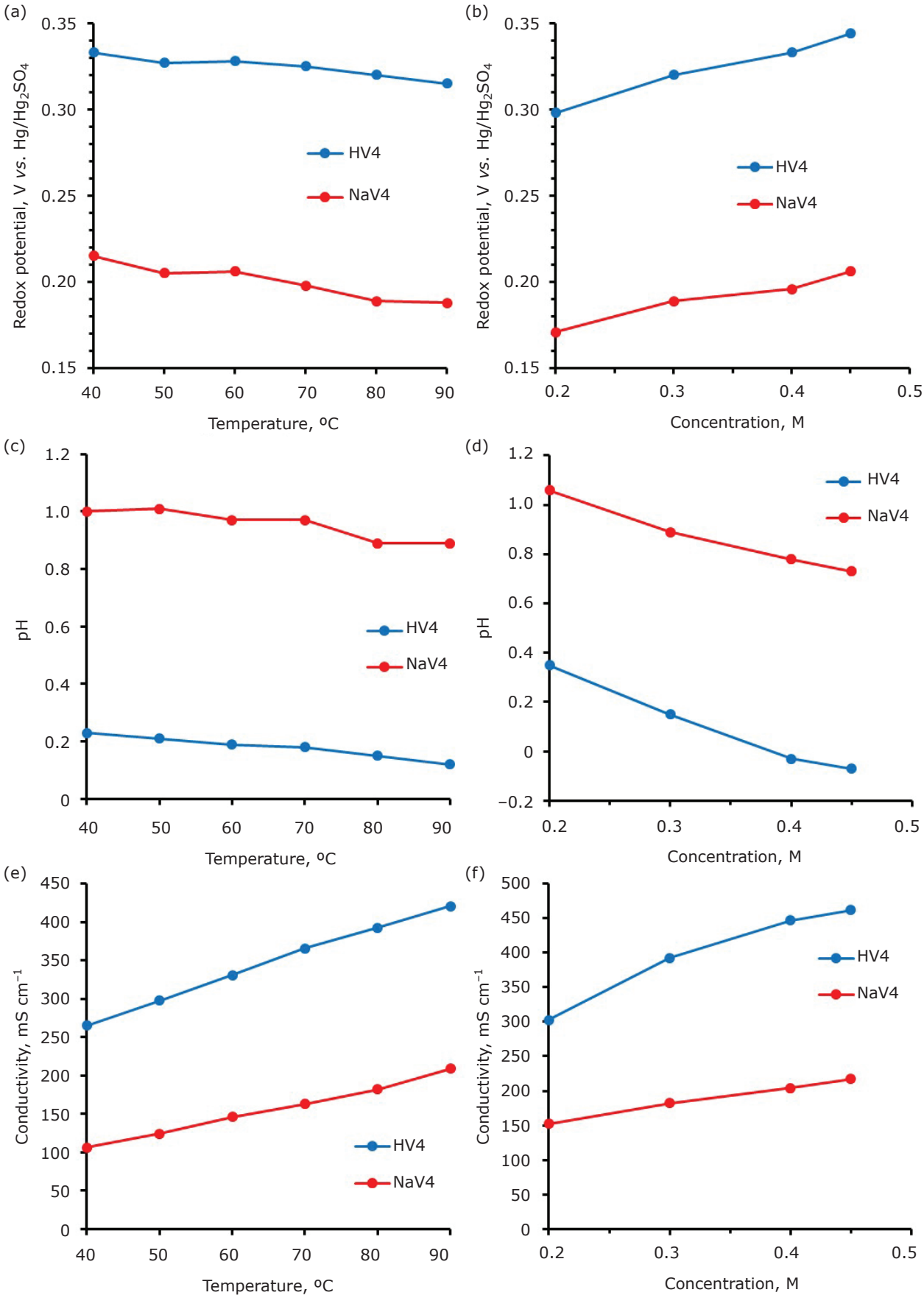

Fig. 3. Thermodynamic properties of 5% reduced HV4 and NaV4 catholytes at: (a), (c) and (e) a range of temperatures for 0.3 M catholyte concentration; and (b), (d) and (f) a range of catholyte concentrations at 80°C

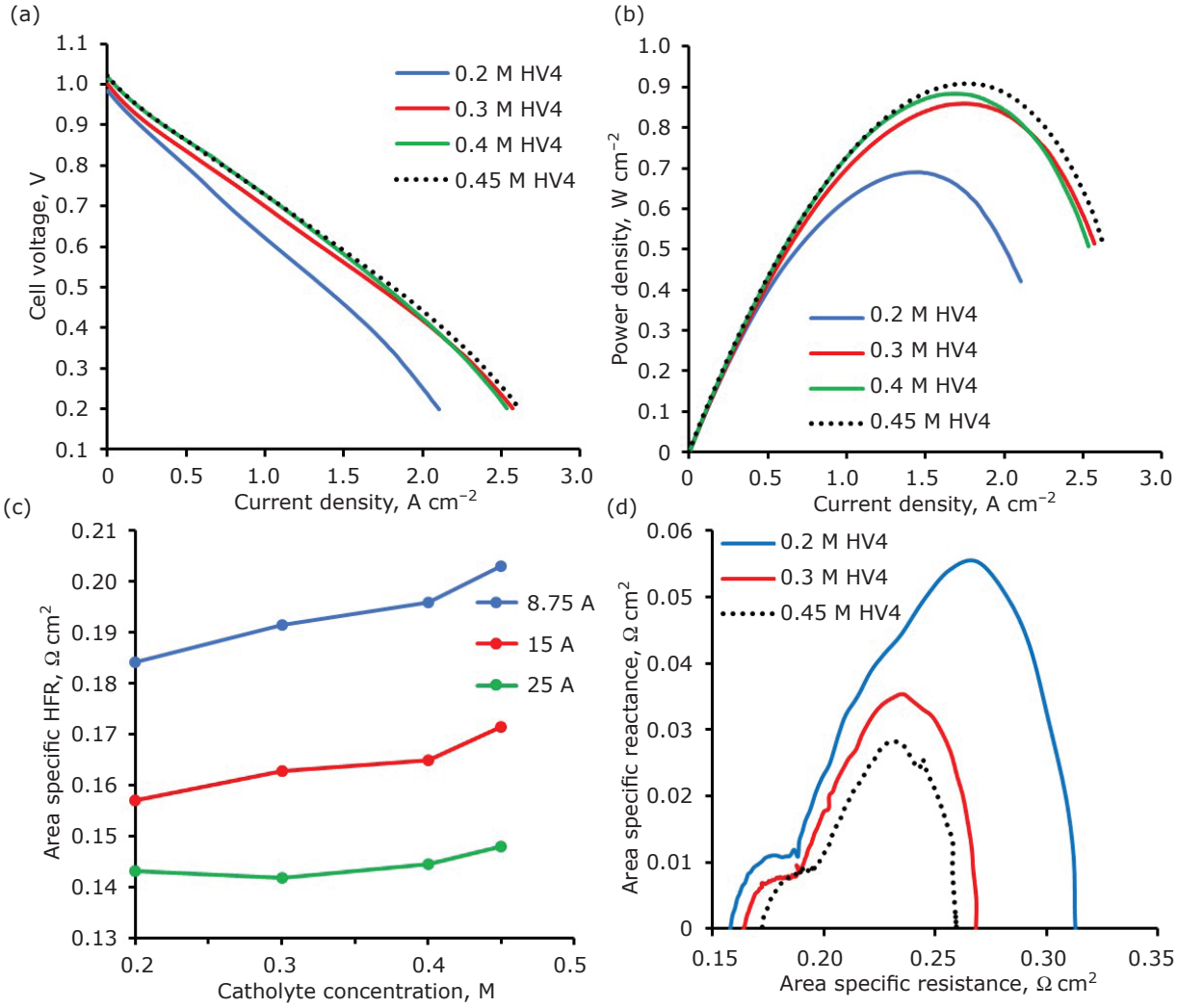

Fig. 4. CRRC fuel cell performance at 80°C: (a) i–V; (b) corresponding power density curves generated with HV4 catholyte at four different concentrations (labelled); (c) high frequency resistance obtained at three current loads for 0.2–0.45 M HV4; (d) Nyquist plots obtained at 0.6 A cm^{-2} for 0.2 M, 0.3 M and 0.45 M HV4

Note, the peak power densities are smaller than the previously reported value of 1.078 W cm^{-2} for 0.3 M HV4 at 80°C because of the thicker membrane (18). The current density-voltage (i–V) curves in **Figure 4(a)** show a considerable improvement in performance on increasing HV4 concentration from 0.2 M to 0.3 M, which translates to a 25% increase in peak power. In addition, there is a noticeable increase in the maximum current density. However, the gains from further increasing catholyte concentration are much smaller, with a 6% increase in peak power achieved for the 0.3→0.45 M transition. Given the latter corresponds to a 50% increase in catholyte cost, the extra power gained may not be economical. In addition, there is little change in the maximum current density on increasing the catholyte concentration from 0.3 M to 0.45 M. This suggests a limiting current was not achieved at 0.2 V for the higher catholyte concentrations and, therefore, the performance of the cell can be considerably improved.

The impedance results in **Figures 4(c)** and **4(d)** provide insights into the cause of the performance benefits gained by increasing concentration. The area specific high frequency resistance (HFR) values obtained at 0.35 A cm^{-2}, 0.6 A cm^{-2} and 1 A cm^{-2} (8.75 A, 15 A and 25 A) in **Figure 4(c)** all show an increase in cell ohmic resistance as the catholyte concentration increases – the opposite of that expected from the conductivity results in **Figure 3(f)**. The reason for this is unclear, but may be linked to VO_2^+ and VO^{2+} species occupying sites within the membrane. The Nyquist plots (at 0.6 A cm^{-2}) in **Figure 4(d)** show the total cell resistance (the low frequency intercept) decreasing with concentration. Although not shown, the larger

arcs on the right were found to vary with catholyte flow rate (the smaller arcs on the left were unaffected), suggesting those arcs are associated with impedance due to catholyte mass transport. Therefore, the left arcs must be related to anode impedance and/or catholyte kinetics. As catholyte concentration increases, there is a sharp decrease in the size of the right arc, consistent with the expected decrease in concentration voltage loss (i.e. cathode mass transport). This is accompanied by a subtle decrease in the left arc, most likely caused by an increase in the cathode exchange current. However, there is also an increase in cell ohmic resistance which diminishes the improvements gained by increasing concentration. As such, increasing the concentration beyond 0.3 M results in relatively minor performance improvements.

The corresponding situation for 5% reduced NaV4 is illustrated in **Figure 5** (the same trends were observed for a range of reduction levels). Note the transient cell performance is poor compared to HV4 due to the large difference in open circuit voltages (18). **Figures 5(a)** and **5(b)** suggest the best cell performance is obtained with 0.3 M NaV4. As before, there is a significant increase in limiting current and peak power density on increasing the NaV4 concentration from 0.2 M to 0.3 M. However, a further increase in concentration has a detrimental

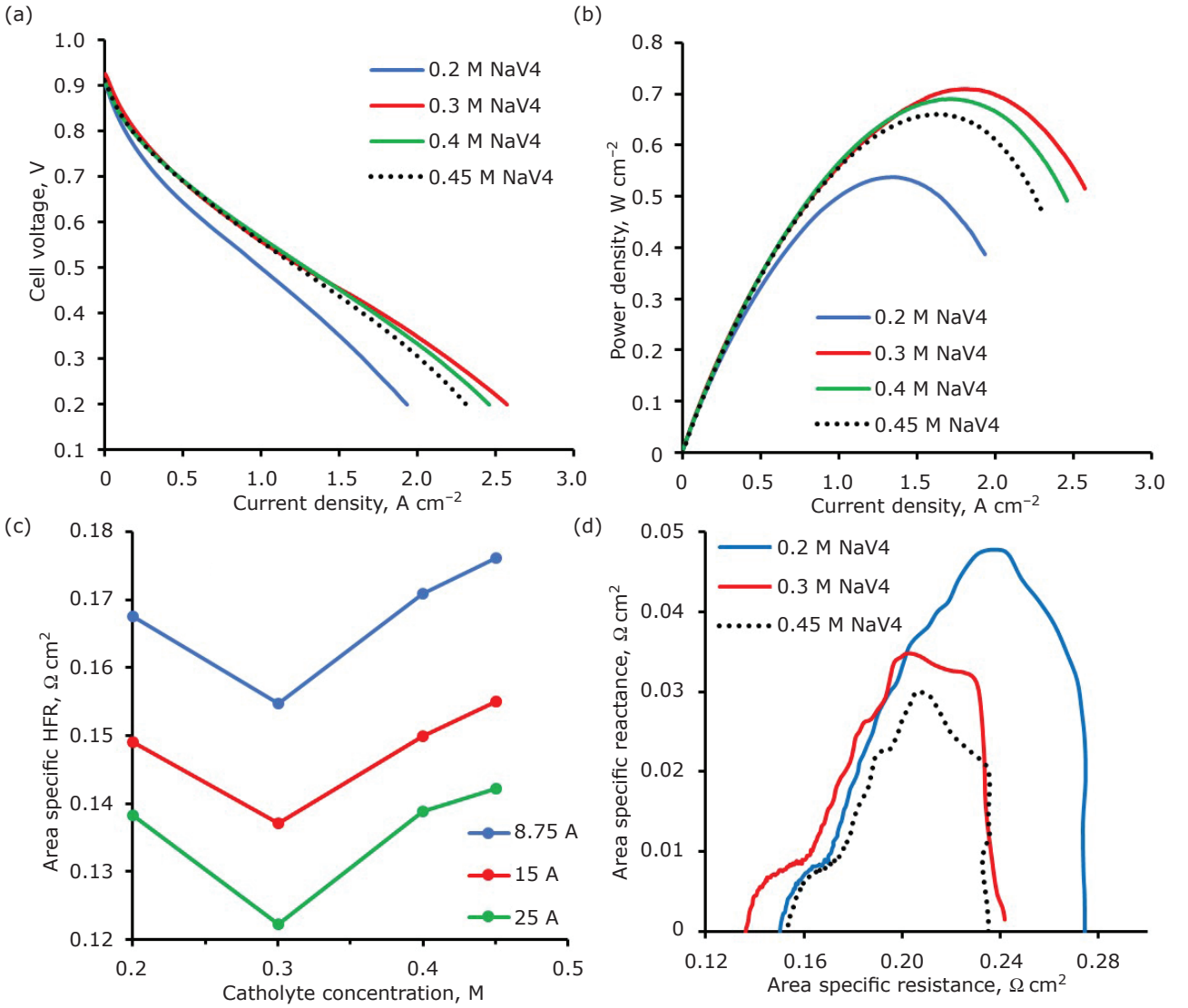

Fig. 5. CRRC fuel cell performance at 80°C: (a) i–V; (b) corresponding power density curves generated with NaV4 catholyte at four different concentrations (labelled); (c) high frequency resistance obtained at three current loads for 0.2–0.45 M NaV4; (d) Nyquist plots obtained at 0.6 A cm^{-2} for 0.2 M, 0.3 M and 0.45 M NaV4

effect on performance. The Nyquist plots in **Figure 5(d)** show the right-hand arc, associated with catholyte mass transport, decreasing in size as catholyte concentration increases, as seen with HV4. However, unlike HV4, the cell ohmic resistance (**Figure 5(c)**) is lowest for the 0.3 M catholyte concentration, leading to the best observed performance. Comparing **Figures 4(c)** and **5(c)**, the increase in HFR from 0.2 M to 0.45 M catholyte concentration is much larger for HV4 than for NaV4. One reason for this could be differing amounts of free vanadium(IV), which could occupy membrane sites, displacing protons. Due to differences in pH, the concentration of VO^{2+} in reduced HV4 will be much larger than NaV4, for the same reduction level (38). Conversely, more vanadium(IV) will be keggin bound (i.e. anionic) in reduced NaV4 than in reduced HV4 (38).

Figures 6(a) and **6(b)** illustrate the effect of temperature on the performance of a CRRC fuel cell using 0.3 M HV4 catholyte (5% reduced). At low current density, the i–V curves show the positive effect of temperature on reaction kinetics, with smaller activation losses as the temperature increases. However, at higher current densities, operation above 80°C has a detrimental effect on performance. For the temperatures studied (40–90°C), the cell peak power density ranges from 692 mW cm^{-2} to 860 mW cm^{-2}, corresponding to a 24% power increase (from 40°C to 90°C). In a

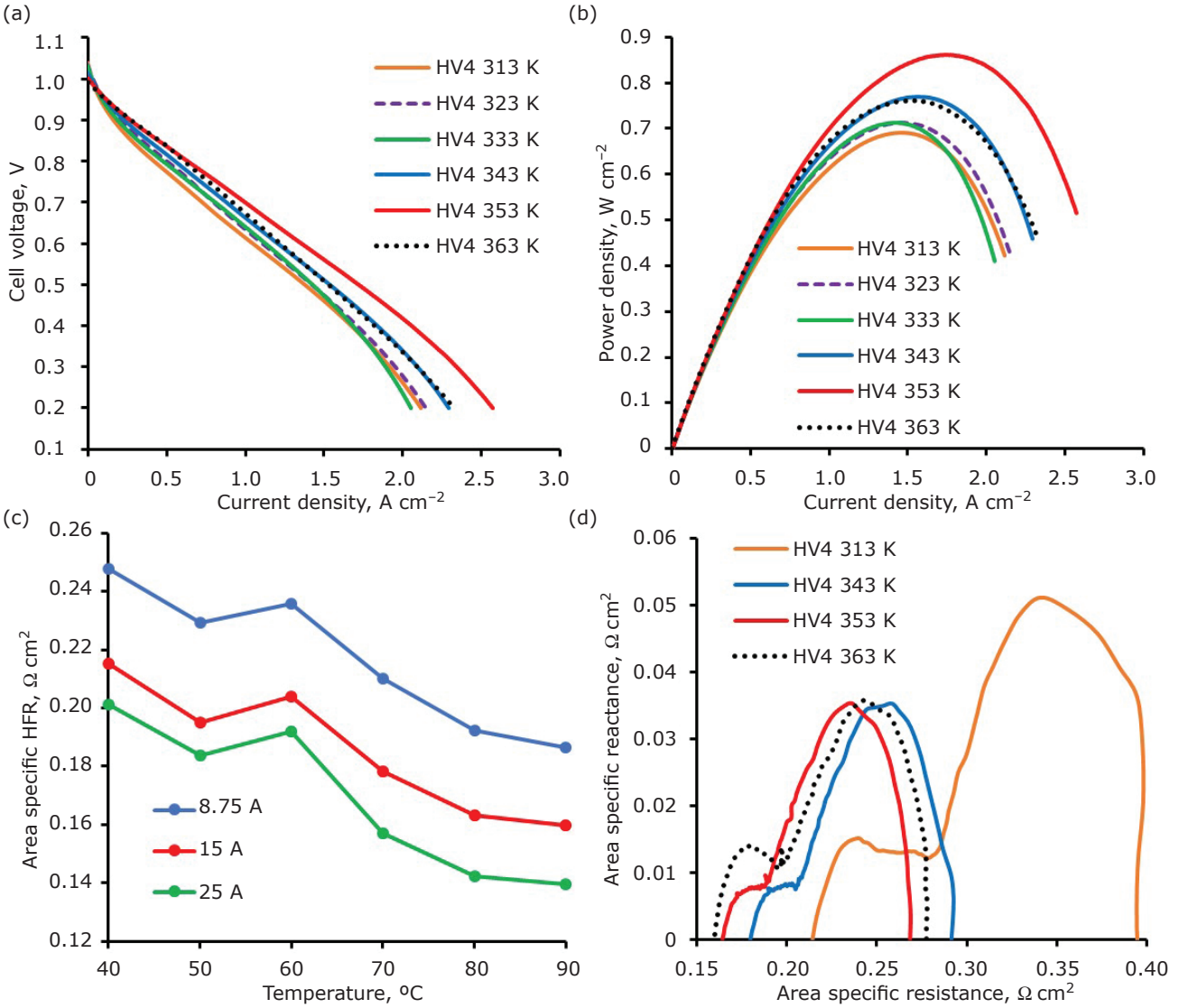

Fig. 6. (a) i–V; (b) corresponding power density curves generated with 0.3 M HV4 catholyte at a range of temperatures (labelled); (c) high frequency resistance obtained at three current loads over a range of temperatures for 0.3 M HV4; (d) Nyquist plots obtained at 0.6 A cm^{-2} over a range of temperatures for 0.3 M HV4

study with a conventional PEFC and fully humidified H_2 and air, Song *et al.* found raising cell temperature from 40°C to 100°C increased peak power from ~500 mW cm^{-2} to ~800 mW cm^{-2}, a 60% increase (25). This suggests the CRRC PEFC in **Figure 6** is quite robust to temperature and cold starts would not be as problematic as in conventional PEFCs.

The HFR results in **Figure 6(c)** show cell ohmic resistance continuously decreases with increasing temperature, even at 90°C. Thus, although the fuel is dry hydrogen, the membrane drying observed in other temperature studies with PEFCs is not present here due to the aqueous cathode (39). Rather, temperature has the expected positive effect on ohmic resistance *via* increasing the ionic conductivity of the electrolytes. The Nyquist plots in **Figure 6(d)** provide insights into the performance trends in **Figures 6(a)** and **6(b)**. As observed, increasing temperature from 40°C to 70°C reduces all three sources of voltage loss: the right-hand arc (catholyte mass transport) and left-hand arc (associated with kinetics) are both dramatically reduced in size and cell ohmic resistance also decreases. On moving from 70°C to 80°C, the two arcs remain similar in shape and size, the main difference being the shift to a lower HFR, hence lower overall cell resistance. However, on increasing to 90°C, there is a significant growth in the left-hand arc, which more than offsets the decrease in HFR. Thus, the overall cell resistance increases and the cell performs worse than at 80°C. Although not shown, the left-hand arc has been found to increase when the anode is poisoned, suggesting anode kinetics can affect its shape. In this case, **Figure 6(d)** would agree with other studies of high temperature conventional PEFCs, where increasing temperature was found to decrease electrochemical Pt surface areas and exchange current densities (25, 40, 41). Thus, high temperature CRRC PEFC performance may be limited by anode kinetics.

The effect of temperature on NaV4 catholyte performance was similar to that for HV4. The power density curves for 0.3 M NaV4 (25% reduced) over a temperature range of 40–90°C are shown in **Figure 7(a)**, along with HFR results in **Figure 7(b)**. As with HV4, 80°C gave the best performance and cell ohmic resistance decreased over the whole temperature range. Thus, no membrane drying was observed and the reduction in performance on moving to 90°C operation can be tentatively attributed to a decrease in the total area of the Pt | electrolyte | hydrogen 3-phase boundary on the anode.

3.4 Regenerator Performance

Following the method of Gunn *et al.* (16), regeneration sweeps were performed with reduced catholytes over the range of conditions in **Table II** (see the Supplementary Information for more details). Using data generated from

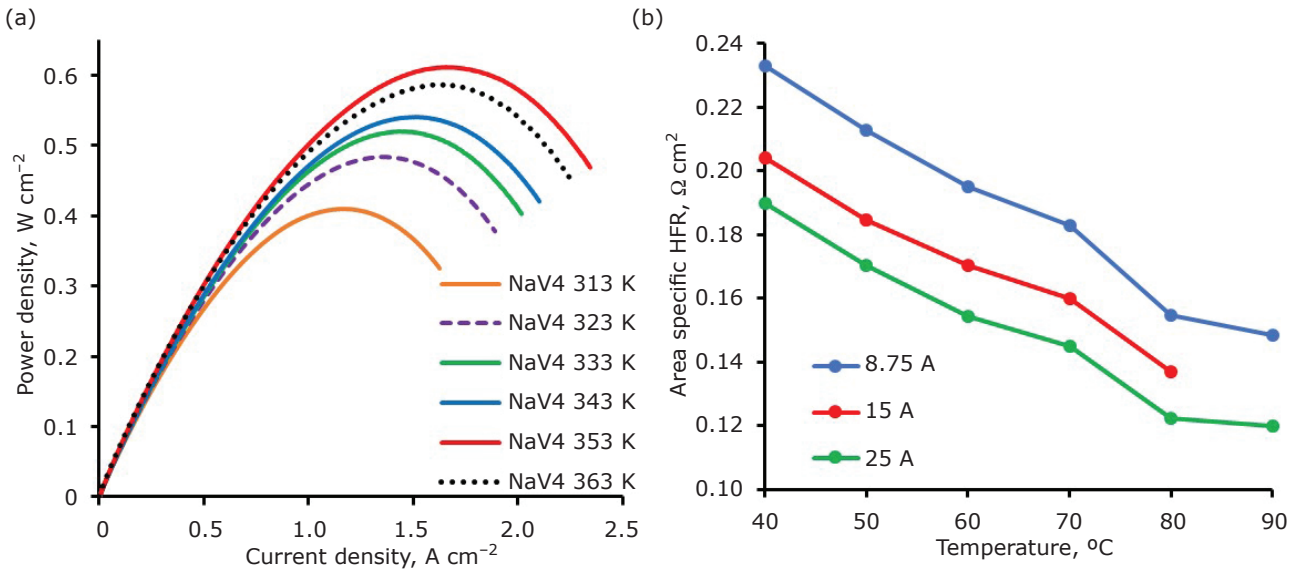

Fig. 7. (a) Current density-power density curves generated with 0.3 M NaV4 catholyte at a range of temperatures (labelled); (b) high frequency resistance obtained at three current loads over a range of temperatures for 0.3 M NaV4

these experiments, the rate of the regeneration reaction (i.e. the rate of vanadium(IV) oxidation) can be expressed as a 'regeneration current' (16). **Figure 8** illustrates regeneration currents evaluated at different reduction levels for HV4 and NaV4 over the concentration/temperature matrix investigated. As observed previously, regeneration currents for NaV4 noticeably exceed those for HV4 (at the same conditions) due to the difference in pH of the two catholytes (18). For both catholytes, concentration has a relatively minor effect on the rate of the regeneration reaction, with varying direction. In general, for high levels of reduction, increasing catholyte concentration has a positive effect on the regeneration current, whereas the opposite occurs for low reduction levels. Increasing temperature appears to benefit catholyte regeneration apart from the fastest reactions (i.e. currents greater than ~35 A) where increasing to 90°C is detrimental.

Zhizhina *et al.* studied the regeneration of 0.2 M $H_7PV_4Mo_8O_{40}$ at various levels of reduction over a range of temperatures (40–90°C) in 1 atm O_2 (37). The researchers used a basic shaking method to mix gas and liquid. The maximum volumetric regeneration current they measured was approximately 400 A l^{-1}, recorded at 90°C for 68% reduced catholyte. This corresponds to ~80 A l^{-1} for the same reaction in air. In the CRRC system, 65% reduced 0.2 M HV4 produced a regeneration current of ~30 A. Given the volume of catholyte in the regenerator is ~250 ml, this corresponds to a

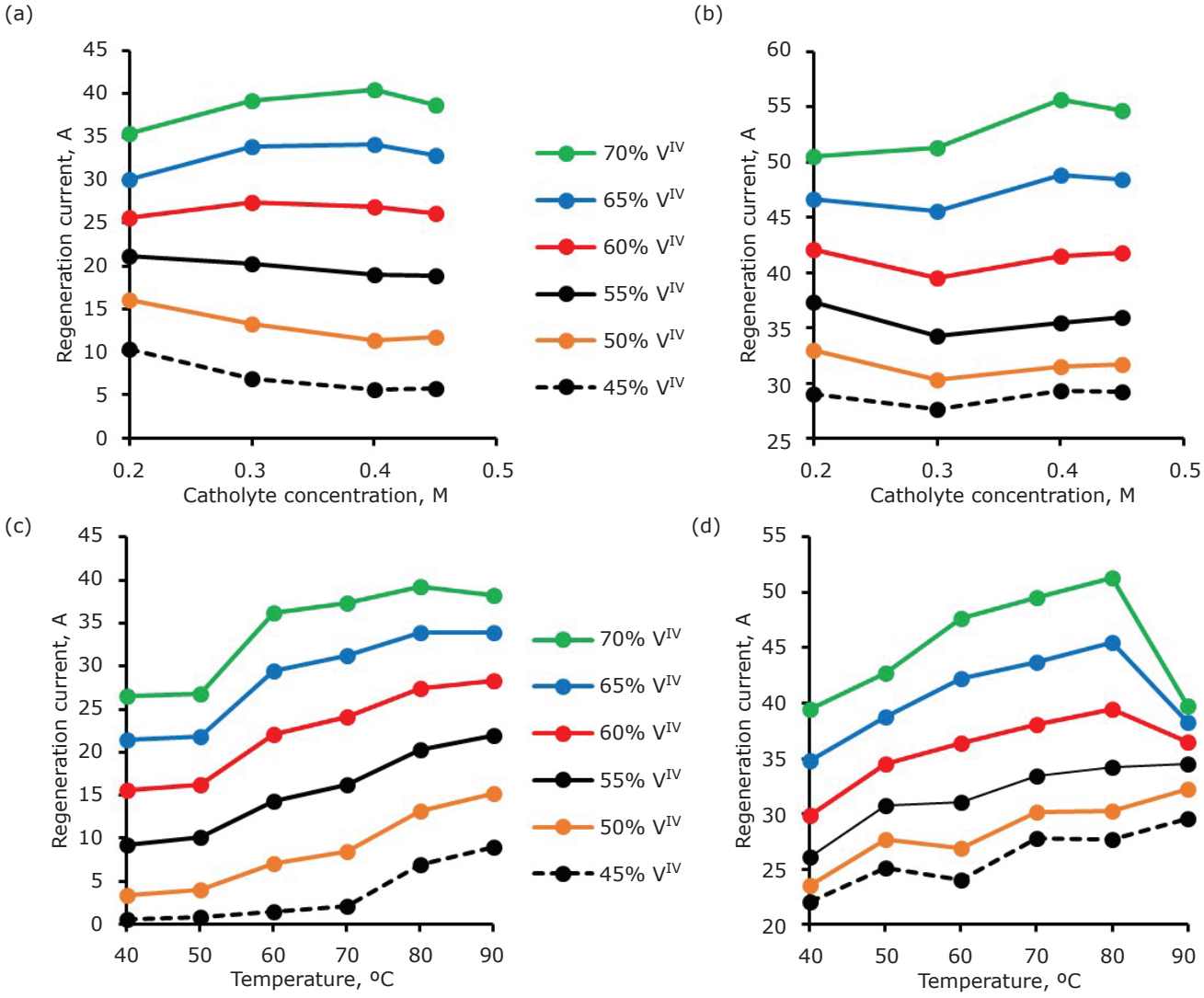

Fig. 8. Regeneration currents for a range of catholyte reduction levels plotted against concentration for: (a) HV4; (b) NaV4 at 80°C. Regeneration currents for a range of catholyte reduction levels plotted against temperature for: (c) 0.3 M HV4; (d) 0.3 M NaV4

volumetric current of ~120 A l^{-1}, which is similar in magnitude to that recorded by Zhizhina *et al*., the increase likely caused by the better liquid-gas mixing (37). For reduction levels greater than 50%, Zhizhina *et al.* found the rate of regeneration, *w*, could be described by Equation (vii), where *k* is an apparent rate constant, $[V^{IV}]$ is the concentration of vanadium(IV) in the reduced catholyte, $[H^+]$ is the concentration of protons, p_{O_2} is the partial pressure of oxygen, *R* is the universal gas constant and *T* is temperature (37).

$$w = k[V^{IV}]^{2.8}[H^+]^{-2.5} p_{O_2} e^{-\frac{10}{RT}} \quad \text{(vii)}$$

Equation (vii) suggests increasing the temperature and concentrations of oxygen and reduced catholyte all have a positive effect on the rate of regeneration, as expected. The negative dependence on proton concentration is less obvious and arises from POM-speciation effects. Only keggin-bound vanadium(IV) can reduce molecular oxygen. Decreasing the pH favours the formation of VO^{2+} (38) and thus, results in slower regeneration kinetics. Equation (vii) also explains the trends in **Figure 8**. Increasing the catholyte concentration for a given reduction level increases both vanadium(IV) and proton concentration (see **Figure 3(e)**). In addition, increasing the reduction level increases catholyte pH. So, the positive effect of increasing catholyte concentration is only observed at the highest reduction levels. Regarding temperature, the trends in **Figures 8(c)** and **8(d)** agree with the exponential term in Equation (vii), apart from some of the results at 90°C. The latter is caused by the effect of temperature on oxygen solubility. When the kinetics are fast, the reaction can be limited by the mass transport of dissolved oxygen. In this case, increasing temperature may have a negative effect on the regeneration rate by decreasing oxygen solubility. This appears to be the case for regeneration currents over 35 A, corresponding to 140 A l^{-1}, at 90°C. Note, this negative effect of temperature was not observed by Zhizhina *et al.* because their (comparative) volumetric currents were significantly lower than 140 A l^{-1} (37).

3.5 Steady State Performance

For many applications, fuel cells are required to perform at a given power for a prolonged time. In this case, transient cell performance results, like those in **Figures 4–7**, are misleading for CRRC PEFCs. The true steady state performance of CRRC PEFC systems is often not reported. It corresponds to the cell operating voltage when the regeneration current equals the cell current. In this case, the redox potential of the catholyte entering the fuel cell does not change, resulting in a constant cell operating voltage (providing the cell is durable). **Figure 9** illustrates the measured steady state cell voltage at 1 A cm^{-2} for both HV4 and NaV4 catholytes at all the conditions in **Table II**. The highest steady state cell voltage of 0.47 V is achieved by 0.45 M NaV4 at 90°C. Reducing the concentration and temperature to 0.3 M and 80°C, respectively, only results in a 10 mV drop in cell voltage, which is tiny considering the difference in cost between 0.3 M and 0.45 M catholyte. Thus, 0.3 M and 80°C appear to be the optimum parameters for NaV4. The same is true for HV4. However, in this case temperature has a greater effect on performance, with much larger variations in cell voltage observed across the matrix of conditions. The reason for this is the relatively low regeneration currents achieved with HV4, making the system more sensitive to temperature. Thus, 0.3 M NaV4 produces better steady state performance than 0.3 M HV4 and is more robust to changes in temperature.

Using the method of Gunn *et al.* (16), the steady state peak power densities were estimated from the transient cell performance and regeneration results for each catholyte in **Table II**. The results are summarised in **Figure 10** and show NaV4 outperforms HV4 at all conditions. For both catholytes at 0.3 M concentration, increasing temperature improves steady state peak power up to 80°C, after which performance diminishes (**Figure 10(a)**). Likewise, **Figure 10(b)** suggests 0.3 M is the optimum temperature for both NaV4 and HV4 catholytes.

4. Conclusions

Although there are subtle differences in how temperature and concentration affect the regenerator and cell performance of HV4 and NaV4 catholytes, in terms of the overall CRRC system, the results are identical: 0.3 M and 80°C result in the optimum steady state performance for both HV4 and NaV4 catholytes (at ambient pressure). No meaningful benefit in system performance can be obtained from further increasing catholyte concentration. Likewise, increasing the temperature beyond 80°C appears to be detrimental for both HV4 and NaV4. Surprisingly, the CRRC PEFCs could operate with dry hydrogen at 90°C and ambient pressure with no evidence of membrane drying.

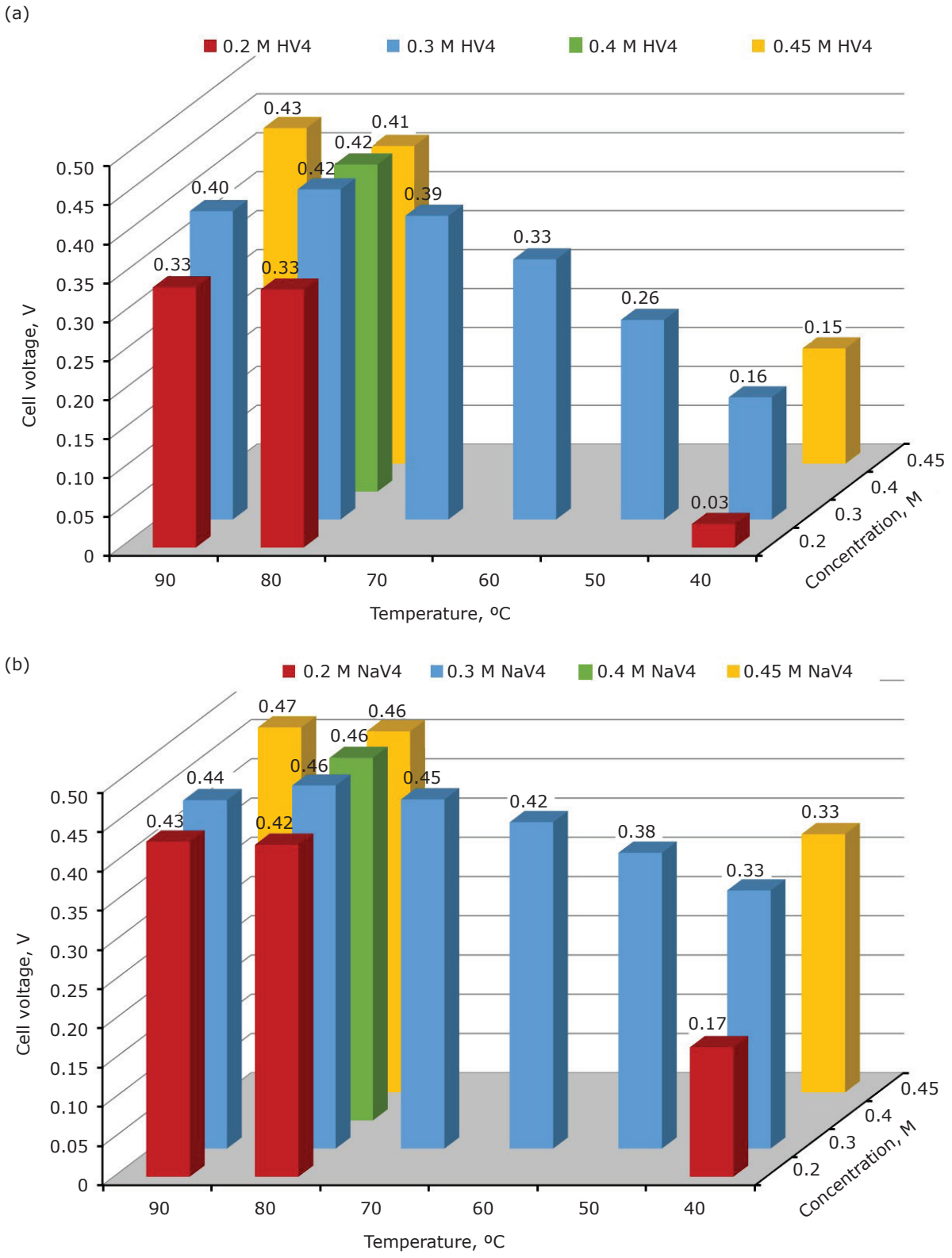

Fig. 9. Measured steady state cell operating voltage at 1 A cm^{-2} for a CRRC fuel cell using: (a) HV4; (b) NaV4 catholytes at a range of concentrations and temperatures

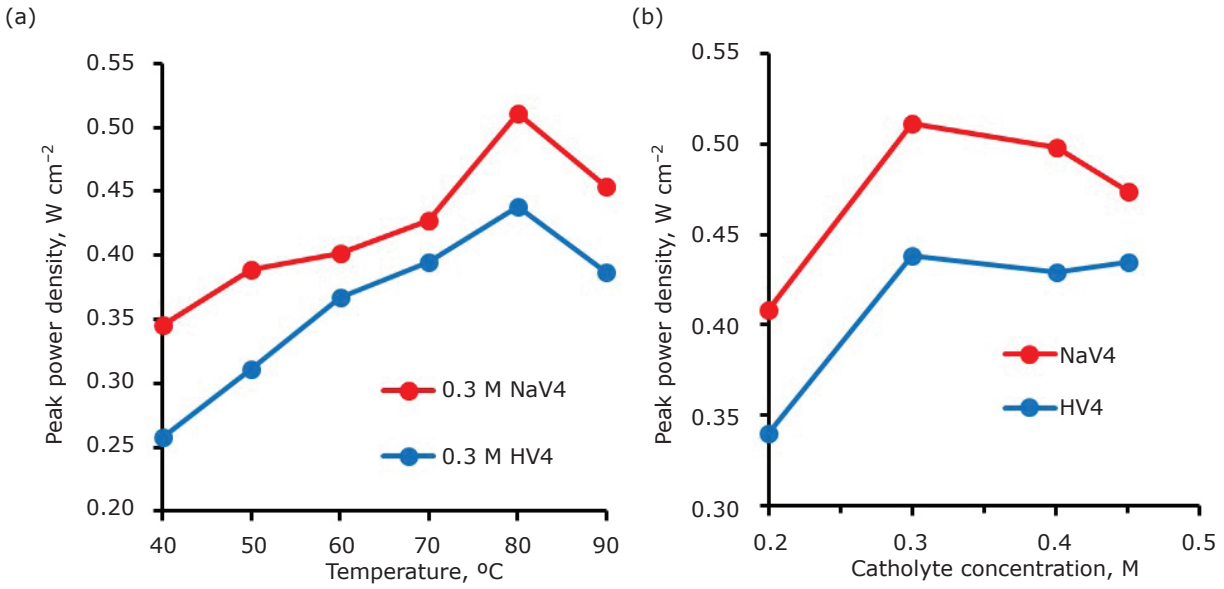

Fig. 10. Estimated steady state peak power densities for a CRRC fuel cell using: (a) 0.3 M HV4 and 0.3 M NaV4 over a range of temperatures; (b) various concentrations of HV4 and NaV4 catholytes at 80°C

However, the step from 80°C to 90°C operation was detrimental for both cell and regenerator performance. The latter was attributed to oxygen solubility issues whilst the former was linked to anode kinetics. Thus, high temperature operation may yield benefits at pressures above 1 atm. This will be explored in future work.

Acknowledgements

This study was part funded by the Higher Education Funding Council for England (HEFCE) Innovation Fund. The authors also thank Dr Corinne Wills (Newcastle University, UK) for the NMR analysis and Dr Natasha Gunn (University of Chester), Dr Matthew Herbert (University of Chester), Joshua Denne (Advanced Propulsion Centre, UK) and Nadine Uwigena (University of Chester) for their help and advice.

References

1. H. A. Gasteiger and N. M. Marković, *Science*, 2009, **324**, (5923), 48
2. M. F. Mathias, R. Makharia, H. A. Gasteiger, J. J. Conley, T. J. Fuller, C. J. Gittleman, S. S. Kocha, D. P. Miller, C. K. Mittelsteadt, T. Xie, S. G. Yan and P. T. Yu, *Electrochem. Soc. Interface*, 2005, **14**, (3), 24
3. T. Yoshida and K. Kojima, *Electrochem. Soc. Interface*, 2015, **24**, (2), 45
4. "Fuel Cells: Data, Facts and Figures", eds. D. Stolten, R. C. Samsun and N. Garland, Wiley-VCH Verlag GmbH & Co KGaA, Weinheim, Germany, 2016, 408 pp
5. 'Germany: H2 MOBILITY Targets 400 Hydrogen Fueling Stations by 2023', Hydrogen Mobility Europe, Fuel Cells and Hydrogen Joint Undertaking, Brussels, Belgium, 5th May, 2016
6. "Fuel Cell Technical Team Roadmap", U.S. DRIVE, Office of Energy Efficiency and Renewable Energy, Washington, DC, USA, June, 2013
7. F. T. Wagner, B. Lakshmanan and M. F. Mathias, *J. Phys. Chem. Lett.*, 2010, **1**, (14), 2204
8. O. T. Holton and J. W. Stevenson, *Platinum Metals Rev.*, 2013, **57**, (4), 259
9. H. A. Gasteiger, S. S. Kocha, B. Sompalli and F. T. Wagner, *Appl. Catal. B: Environ.*, 2005, **56**, (1–2), 9
10. F. D. Coms, *ECS Trans.*, 2008, **16**, (2), 235
11. E. Endoh, S. Terazono, H. Widjaja and Y. Takimoto, *Electrochem. Solid-State Lett.*, 2004, **7**, (7), A209
12. C. A. Reiser, L. Bregoli, T. W. Patterson, J. S. Yi, J. D. Yang, M. L. Perry and T. D. Jarvi, *Electrochem. Solid-State Lett.*, 2005, **8**, (6), A273
13. E. Brightman and G. Hinds, *J. Power Sources*, 2014, **267**, 160
14. Yu. V. Tolmachev and M. A. Vorotyntsev, *Russ. J. Electrochem.*, 2014, **50**, (5), 403
15. A. M. Posner, *Fuel*, 1955, **34**, 330
16. N. L. O. Gunn, D. B. Ward, C. Menelaou, M. A. Herbert and T. J. Davies, *J. Power Sources*, 2017, **348**, 107

17. R. Singh, A. A. Shah, A. Potter, B. Clarkson, A. Creeth, C. Downs and F. C. Walsh, *J. Power Sources*, 2012, **201**, 159
18. D. B. Ward, N. L. O. Gunn, N. Uwigena and T. J. Davies, *J. Power Sources*, 2018, **375**, 68
19. S.-B. Han, D.-H. Kwak, H. S. Park, I.-A. Choi, J.-Y. Park, K.-B. Ma, J.-E. Won, D.-H. Kim, S.-J. Kim, M.-C. Kim and K.-W. Park, *ACS Catal.*, 2016, **6**, (8), 5302
20. S.-B. Han, D.-H. Kwak, H. S. Park, I.-A. Choi, J.-Y. Park, S.-J. Kim, M.-C. Kim, S. Hong and K.-W. Park, *Angew. Chem. Int. Ed.*, 2017, **56**, (11), 2893
21. '3.4: Fuel Cells, 2016', in "Fuel Cell Technologies Office Multi-Year Research, Development, and Demonstration Plan", Office of Energy Efficiency and Renewable Energy, Washington, DC, USA, May, 2017
22. 'ACAL Energy Fuel Cell Achieves 10,000 Hour Endurance', Fuel Cell Today, Royston, Hertfordshire, UK, 27th June, 2013
23. V. F. Odyakov, E. G. Zhizhina and K. I. Matveev, *J. Mol. Catal. A: Chem.,* 2000, **158**, (1), 453
24. T. Matsui, E. Morikawa, S. Nakada, T. Okanishi, H. Muroyama, Y. Hirao, T. Takahashi and K. Eguchi, *ACS Appl. Mater. Interfaces*, 2016, **8**, (28), 18119
25. C. Song, Y. Tang, J. L. Zhang, J. Zhang, H. Wang, J. Shen, S. McDermid, J. Li and P. Kozak, *Electrochim. Acta*, 2007, **52**, (7), 2552
26. C. Zhang, T. S. Zhao, Q. Xu, L. An and G. Zhao, *Appl. Energy*, 2015, **155**, 349
27. F. A. de Bruijn, R. C. Makkus, R. K. A. M. Mallant and G. J. M. Janssen, *Adv. Fuel Cells*, 2007, **1**, 235
28. N. Martin and M. Herbert, ACAL Energy Ltd, 'Synthesis of Polyoxometalates', *World Patent Appl.* 2015/097,459
29. L. Pettersson, *Mol. Eng.*, 1993, **3**, (1–3), 29
30. L. Pettersson, I. Andersson, J. H. Grate and A. Selling, *Inorg. Chem.*, 1994, **33**, (5), 982
31. A. Selling, I. Andersson, J. H. Grate and L. Pettersson, *Eur. J. Inorg. Chem.*, 2000, (7), 1509
32. I. V. Kozhevnikov, *Chem. Rev.*, 1998, **98**, (1), 171
33. P. Souchay, F. Chauveau and P. Courtin, *Bull. Soc. Chim. France*, 1968, (6), 2384
34. I. V. Kozhevnikov, *Izv. Akad. Nauk SSSR: Ser. Khim.*, 1983, **4**, 721; translated into English in *Russ. Chem. Bull*., 1983, **32**, (4), 655
35. V. M. Berdnikov, L. I. Kuznetsova, K. I. Matveev, N. P. Kirik and E. N. Yurchenko, *Koord. Khim.*, 1979, **5**, (1), 78
36. I. V. Kozhevnikov, Yu. V. Burov and K. I. Matveev, *Izv. Akad. Nauk SSSR: Ser. Khim.*, 1981, **11**, 2428; translated into English in *Russ. Chem. Bull*., 1981, **30**, (11), 2001
37. E. G. Zhizhina, V. F. Odyakov, M. V. Simonova and K. I. Matveev, *Kinet. Catal.*, 2005, **46**, (3), 354
38. A. Selling, I. Andersson, J. H. Grate and L. Pettersson, *Eur. J. Inorg. Chem.*, 2002, (3), 743
39. L. Wang, A. Husar, T. Zhou and H. Liu, *Int. J. Hydrogen Energy*, 2003, **28**, (11), 1263
40. J. Zhang, Y. Tang, C. Song, J. Zhang and H. Wang, *J. Power Sources*, 2006, **163**, (1), 532
41. Y. Song, J. M. Fenton, H. R. Kunz, L. J. Bonville and M. V. Williams, *J. Electrochem. Soc.*, 2005, **152**, (3), A539

The Authors

David B. Ward is a Leading Research Fellow at the University of Chester, UK. His interests lie in the study and development of environmentally considerate engineering technologies and practices. David graduated in 2001 with a PhD from the Department of Chemical and Process Engineering, University of Sheffield, UK. He spent several years working as a Senior Engineer for a research and development (R&D) start-up, ACAL Energy Ltd, developing a high efficiency gas liquid oxidation reactor for a novel hydrogen proton exchange membrane (PEM) fuel cell engine. David continues to advance this work with respect to both fuel cells and water treatment applications.

Trevor J. Davies was a Senior Lecturer at the University of Chester and led the Electrochemistry Research Group from 2014 to 2018. His research interests include electrolysers, fuel cells, flow batteries and sensors. Trevor completed his PhD in Chemistry in 2005 at the University of Oxford, UK. Before joining Chester in 2014, he was a fuels scientist at Shell, UK, and subsequently led the cathode development programme at ACAL Energy Ltd, UK. Trevor recently left the University of Chester to join INOVYN's Electrochemical Technology Business.

